MRI vs. US 3D computational models of carotid arteries: a proof-of-concept study

Panagiotis K. Siogkas, Vassilis D. Tsakanikas, Antonis I. Sakellarios, Vassiliki T. Potsika
Unit of Medical Technology and Intelligent Information Systems, Department of Materials Science and Engineering
University of Ioannina
Ioannina, Greece
psiogkas4454@gmail.com, vasilistsakanikas@gmail.com, ansakel13@gmail.com, vpotsika@gmail.com

George Galyfos, Fragiska Sigala
First Propedeutic Department of Surgery
National and Kapodistrian University of Athens
Athens, Greece
georgegalyfos@hotmail.com, drfsigala@yahoo.gr

Igor Koncar
Department of Vascular and Endovascular Surgery, Faculty of Medicine
University of Belgrade
Belgrade, Serbia
dr.koncar@gmail.com

Smiljana Tomašević, Tijana Djukic, Nenad Filipovic
Faculty of Engineering
University of Kragujevac
Kragujevac, Serbia
smiljana2705@gmail.com, tijana@kg.ac.rs, fica@kg.ac.rs

Dimitrios I. Fotiadis
Unit of Medical Technology and Intelligent Information Systems, Department of Materials Science and Engineering
University of Ioannina
University of Ioannina
Ioannina, Greece
fotiadis@uoi.gr

***Abstract*— The progression of atherosclerotic carotid plaque causes a gradual stenosis in the arterial lumen which might result to catastrophic plaque rupture ending to thromboembolism and stroke. Carotid artery disease is the main cause for ischemic stroke in the EU, thus intensifying the need of the development of tools for risk stratification and patient management in carotid artery disease. In this work, we present a comparative study between ultrasound-based and MRI-based 3D carotid artery models to investigate if US-based models can be used to assess the hemodynamic status of the carotid vasculature compared with the respective MRI-based models which are considered as the most realistic representation of the carotid vasculature. In-house developed algorithms were used to reconstruct the carotid vasculature in 3D. Our work revealed a promising similarity between the two methods of reconstruction in terms of geometrical parameters such as cross-sectional areas and centerline lengths, as well as simulated hemodynamic parameters such as peak Time-Averaged WSS values and areas of low WSS values which are crucial for the hemodynamic status of the cerebral vasculature. The aforementioned findings, therefore, constitute carotid US a possible MRI surrogate for the initial carotid artery disease assessment in terms of plaque evolution and possible plaque destabilization.**

Keywords—computational models, carotid, ultrasound, MRI, blood flow simulations

I. INTRODUCTION

One of the most well-known causes of death in the EU resulting to 440,000 deaths per year is stroke. Besides death, stroke is mainly responsible for major disabilities in adults with more than one out of two stroke survivors resulting in being totally dependent on other people for everyday simple activities. The total annual costs that are linked to stroke reach the insane amount of almost €45 billion which includes both direct and indirect costs for productivity loss and health care [1, 2].

One of the most critical causes of stroke is the progression of carotid artery disease which results in enlarged atheromatic plaques which can be prone to erosion or rupture. The rupture of the atheromatic plaques results to thromboembolism and finally, cerebral infarction. Interestingly enough, stenoses larger than 50% from asymptomatic plaques within the internal carotid artery (ICA) result to thromboembolisms that are the cause of more than 10% of all strokes. This intensifies the need of novel risk stratification tools which will improve patient management in cases of moderate to severe carotid artery disease.

In this context, a large number of studies on modelling the biological processes that are connected to atherosclerosis and simulating the progression of atheromatic plaques have been published [3-7]. The vast majority of these studies are based on idealized 2D carotid models and only a small number of studies have utilized patient-specific 3D arterial models. Patient-specific 3D arterial models can be created utilizing either Computed Tomography (CT) images, Magnetic Resonance Angiography (MRA) images or UltraSound (US) images, respectively. The 3D models (lumen, outer wall and plaque components) are then used to calculate important hemodynamic factors such as Endothelial Shear Stresses (ESS), Plaque Structural Stress (PSS) and identify areas of low ESS, which, in turn, are used to simulate the infiltration of lipoproteins and inflammatory cells within the layers of the arterial wall, a process that favors the progression of atheromatic plaque.

In this work, we present a proof-of-concept study which tries to provide a comparison between MRI-based and US-based 3D carotid arterial models for three patients with a >50% degree of stenosis. The 3D reconstruction of the models was performed using in-house developed algorithms and results on peak time-averaged ESS (TAESS), areas of low ESS, qualitative assessment of the areas of peak ESS and geometrical measurements are presented.

II. MATERIALS AND METHODS

A. Cardiovascular MR and US image acquisition protocols

Three patients with >50% carotid stenosis using a 1.5-T whole-body system (Signa HDx, GE Healthcare, Waukesha, WI, USA) with a bilateral four-channel phased-array carotid coil (Machnet BV, Eelde, the Netherlands) from the TAXINOMISIS cohort were used in the current study. Patient provided written informed consent and enrolled in the TAXINOMISIS clinical study (www.clinicaltrials.gov; ID: NCT03495830) protocol which was approved by the local competent ethics committee. The acquisition settings for the MRI sequences were the following: (i) TOF images: repetition time: 23 ms, effective echo time: 3.2 ms, field of view [FOV]: 160 mm, section thickness: 1 mm; (ii) fast-spin echo double-inversion recovery prepared sequences (T1W): repetition

time: 1428.57 ms, effective echo time: 7.672 ms, FOV: 100 mm, section thickness: 3 mm; (iii) (T2W): repetition time: 1379.31 ms, effective echo time: 99.74 ms, FOV: 100 mm, section thickness: ≤ 2.5 mm (iv) (PDW): repetition time: 1379.31 ms, effective echo time: 7.67 ms, FOV: 100 mm, section thickness: ≤ 2.5 mm. The acquired data were stored in DICOM format. The US transversal and longitudinal images from the carotid bifurcations of interest were acquired from a GE Healthcare LOGIQE9 scanner.

B. 3D reconstruction of the carotid artery using US

The methodology applied to perform the 3D reconstruction of patient-specific carotid artery from US images has presented in literature [8, 9]. The process can be divided in two steps. The first step involves deep learning techniques (more precisely the convolutional neural networks) to perform the segmentation of the US images and the automated extraction of the lumen and wall segments, from both longitudinal and transversal images. The second step involves using the segmented lumen and wall contours to perform automated 3D reconstruction. The longitudinal contours are used to extract the centerline of the vessel as well as information about diameters along the centerline, while transversal contours are used to define the shapes of the cross-sections along the centerline. All this data is represented as a set of B-spline curves and NURBS surfaces, that are further used in the meshing process to obtain the final geometry of the patient-specific carotid artery.

C. 3D reconstruction of the carotid artery and plaque tissue components using MRI

The 3D carotid arterial model reconstruction process is based on a series of magnetic resonance images (MRI), including ToF, T1w, T2w and PD series. Briefly, the TOF sequence is utilized for the reconstruction of the lumen, while the fusion of T1w, T2w and PD series are utilized for the reconstruction of the arterial wall model, as well as the model of the plaque components. The three models are aligned in a later phase for the creation of the final arterial model. The reconstruction process is based on a novel methodology which comprises three steps:

1. **Segmentation of the region of interest**. For segmenting the regions of interest (lumen, outer wall and plaque components), three deep learning models have been created. More specifically, two experts have annotated 485 tuples of ToF, T1w, T2w and PD images from 42 different patients. This process resulted in a training dataset which was used to train three UNET models for the aforementioned region of interest.
2. **3D level set**. A morphological operator is applied to the 3D volume of the stacked 2D segmented frames in order to produce the 3D surface model.
3. **3D meshing**. Marching cubes algorithm is applied to the 3D surface model, resulting to the final reconstructed arterial model. Figure 1 depicts the six 3D reconstructed models that were used in the study.

D. Blood flow simulations

Blood flow simulations were carried out for all six models (three MRI-based and 3 US-based). The same boundary conditions were used for every couple of arterial models. Patient-specific boundary conditions were used for each couple. At the inlet, the patient specific mean arterial pressure (MAP) was used, deriving from the systolic (SBP) and diastolic blood pressure (DBP) measurements that were recorded. MAP was calculated as [10]:

$$MAP = \frac{SBP + 2(DBP)}{3}. \quad (1)$$

Regarding the outlets (i.e., ICA and ECA), patient-specific mass flow rates were used as outlet boundary conditions. The mass flow rate profiles were calculated from the patient- and artery-specific flow velocity measurements which were acquired from the respective US images. In order to avoid inaccuracies at the mass flow rate calculations, the 3D models were trimmed in order to avoid any side branches after the bifurcation site, a fact that would affect the flow distribution within the artery of interest.

In order to model blood flow in our simulations, we used the Navier-Stokes and the continuity equations:

$$\rho \frac{\partial \mathbf{v}}{\partial t} + \rho(\mathbf{v} \bullet \nabla)\mathbf{v} - \nabla \bullet \boldsymbol{\tau} = 0, \quad (2)$$

$$\nabla \bullet (\rho \mathbf{v}) = 0, \quad (3)$$

where $\mathbf{v}$ is the blood velocity vector and $\boldsymbol{\tau}$ is the stress tensor, which is defined as:

$$\boldsymbol{\tau} = -p\delta_{ij} + 2\mu\varepsilon_{ij}, \quad (4)$$

where δ_{ij} is the Kronecker delta, μ is the blood dynamic viscosity, p is the blood pressure and ε_{ij} is the strain tensor calculated as:

$$\varepsilon_{ij} = \frac{1}{2}\left(\nabla \mathbf{v} + \nabla \mathbf{v}^T\right). \quad (5)$$

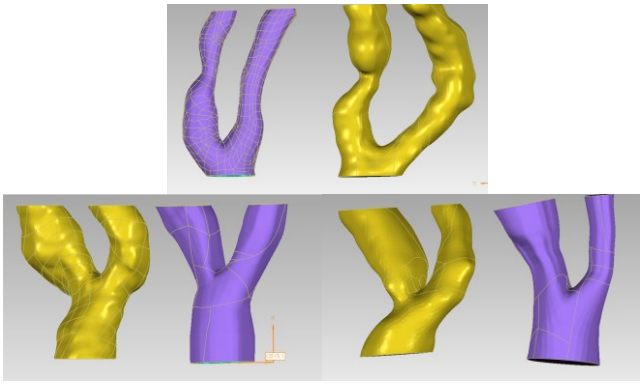

Figure 1. 3D reconstructed models for all three cases. The US-derived 3D models are depicted in purple, whereas the MRI-derived 3D models are depicted in yellow, respectively.

The arterial wall was considered as rigid and impermeable. Blood was treated as Newtonian with density 1050 kg/m^3 and dynamic viscosity 0.0035 Pa·s, respectively. A full cardiac cycle was used in all cases. The duration of each cycle was calculated based on the patient-specific pulse rate and was calculated as 60/pulse rate. Each cycle was divided into timesteps of 0.05 sec in order to achieve better accuracy and convergence. All simulations were carried out using ANSYS® v16.2. The element size was set to 0.16 mm or lower and constituted only of tetrahedra. The convergence criterion was set to 10^{-4} and the iteration limit was 150 for each timestep. Time-averaged ESS values, the ratio of total area of low ESS (i.e., <2 Pa) to the total vessel area and flow velocities were calculated for each model. Furthermore, geometrical parameters such as minimum lumen area (i.e.,

stenosis region), inlet, ICA and ECA area are also calculated for the comparison.

III. RESULTS

The first analysis was based on geometrical findings mainly. We focused on the area of the inlet and the two outlets respectively. Table 1 depicts the calculated areas for the inlet and the outlets for each 3D model, respectively.

Table 1: Inlet and outlet areas for all 3D reconstructed models.

Case ID	CCA area	ICA area	ECA area
040_US	37.5 mm^2	24.8 mm^2	6.1 mm^2
040_MRI	38.6 mm^2	26.6 mm^2	7.1 mm^2
045_US	36.2 mm^2	6.42 mm^2	11.8 mm^2
045_MRI	35.4 mm^2	11.6 mm^2	15.5 mm^2
049_US	41.7 mm^2	27.8 mm^2	15.5 mm^2
049_MRI	46.6 mm^2	23.7 mm^2	22.1 mm^2

Table 2: Blood flow simulations results for all 3D models.

Case ID	Peak ESS at stenosis	Area of low ESS (<2 Pa)/Total Vessel Area (%)
040_US	25.7 Pa	15.3
040_MRI	36 Pa	8.2
045_US	71.2 Pa	19.5
045_MRI	70.4 Pa	13.3
049_US	56.2 Pa	16
049_MRI	46.3 Pa	13.2

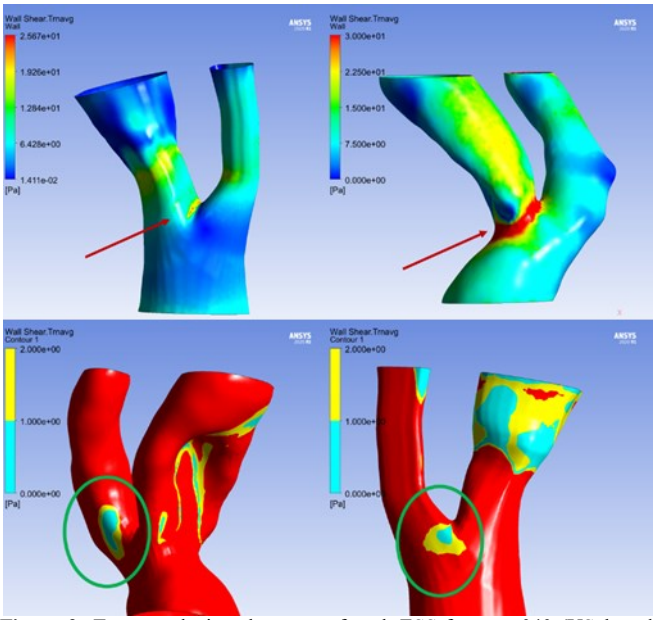

Figure 2: Top row depicts the areas of peak ESS for case 040 (US_based model on the left and MRI_based model on the right), whereas the bottom row depicts areas of low ESS for the same case (US_based model on the right and MRI_based model on the left), respectively.

Following the geometrical analysis, we then performed a comparison in terms of crucial hemodynamic parameters such as peak TAESS and areas of low ESS, respectively. Table 2 contains the calculated values of the aforementioned parameters for all 3D models. Another important factor that was examined was the location of areas of low or peak TAESS values. Briefly, the areas of low ESS matched the two models in terms of location. The same trend was observed for the location of the peak ESS values, which were generally present either at the throat of the existing stenoses or at the bifurcation site. Figures 2, 3 and 4 depict the areas of low ESS and the ESS distribution of all models in pairs (i.e., US-based and MRI-based for each case).

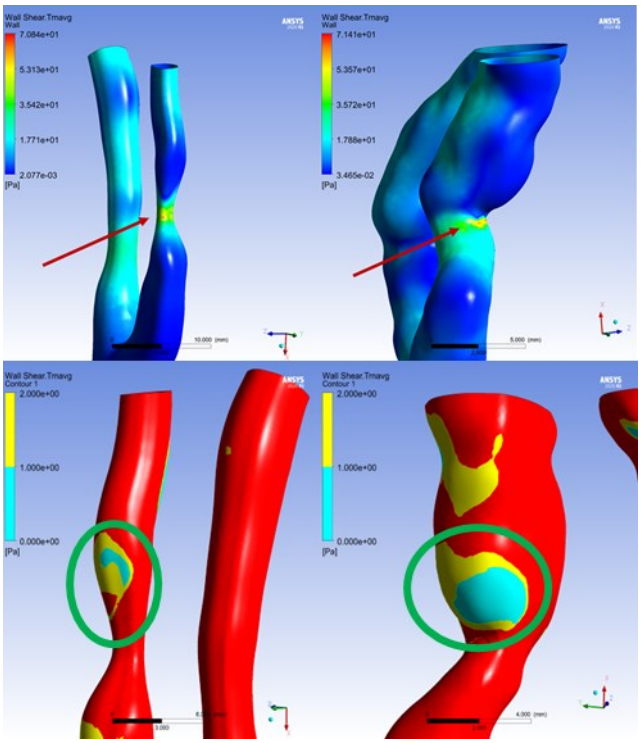

Figure 3: Top row depicts the areas of peak ESS for case 045 (US_based model on the left and MRI_based model on the right), whereas the bottom row depicts areas of low ESS for the same case (US_based model on the left and MRI_based model on the right), respectively.

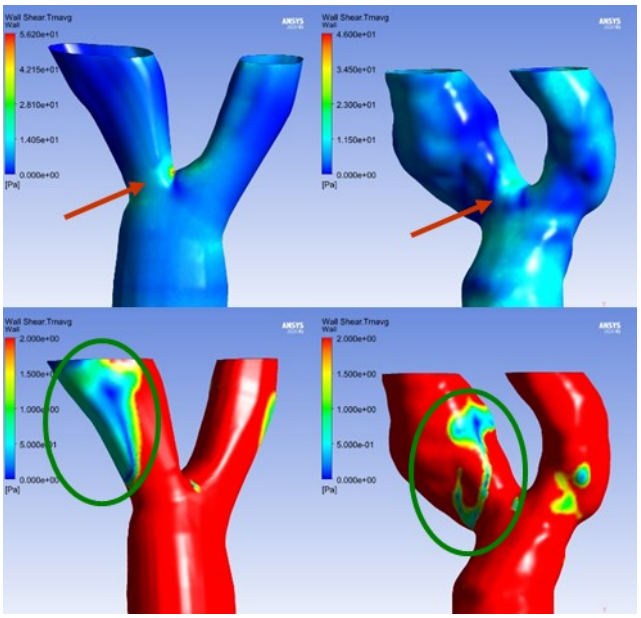

Figure 4: Top row depicts the areas of peak ESS for case 049 (US-based model on the left and MRI-based model on the right), whereas the bottom row depicts areas of low ESS for the same case (US-based model on the left and MRI-based model on the right), respectively.

IV. DISCUSSION

In this proof-of-concept study, we presented a comparison of the 3D models that derived from two important carotid imaging modalities, US and MRI. A geometrical comparison was initially done in order to examine how the two models correlate in terms of diameters at the distal parts of the artery and then, using the same patient-specific boundary conditions for each case, finite element-based blood flow simulations were carried out to investigate the similarity of the calculated hemodynamic parameters such as TAESS and areas of low ESS, respectively. In terms of geometrical similarity, the diameters of the vessels presented with moderately close values. However, due to the nature of US, the surface details of the final US-based 3D models were evidently lower compared to the MRI-based models. This is something that was expected, since US does not provide the amount of information that can be derived from the MRI sequences. Furthermore, the US-based models were much smoother than the MRI-based ones, resulting to a more linearized flow which in turn, produced lower ESS values than the MRI-based models, thus justifying the larger low TAWSS areas. Another important finding is that the location of the areas of low ESS matched the two modalities moderately, which is quite promising. Moreover, the same applies to the sites that exhibited the peak ESS values for each case, a fact that can lead us to the assumption that we observed a fair qualitative match for the ESS distribution throughout the examined vessels. These findings are quite promising, since US is a totally non-invasive imaging modality with minimal patient distress, especially when compared to the strenuous MRI examination, which, if performed using an extended acquisition protocol (i.e., pre and post contrast sequences), can last almost 60-90 minutes. Moreover, US requires far less preparation, it is much easier for the clinician and the examination cost is evidently inferior. However, the limited dataset that was used for the current study does not allow us to draw concrete conclusions on whether US can be used to assess the hemodynamic status of a carotid artery. Furthermore, in order to perform a detailed 3D reconstruction using only US images, an extended acquisition protocol must be followed that will include the common carotid and both the internal and external carotids for an adequate length in both longitudinal and transversal views. This is a crucial parameter for an accurate 3D reconstruction from US images to be feasible. The next step is to extend the dataset to draw more concrete results. If the results of the extended comparison follow the trend of the current work, then US-derived 3D models will be able to be used for flow analysis and provide crucial results to the risk stratification tool that is being developed in the context of the TAXINOMISIS study.

V. CONCLUSION

We present a comparison study between US-based and MRI-based 3D carotid models in three cases with moderate to severe degree of stenosis (>50%). The calculated results revealed that US-derived 3D models can be used for an initial assessment of the hemodynamic status of the carotid vasculature and can point to the areas that are either prone to develop atherosclerotic plaque or areas that exhibit high ESS values and can lead to the destabilization of the already existing plaque. Further analysis must be done in a much larger dataset to establish the respective risk thresholds for the US models so that they can be used at a wider level in clinical practice.

ACKNOWLEDGMENT

This work has received funding from the European Union's Horizon 2020 research and innovation programme under grant agreement No 755320, as part of the TAXINOMISIS project.

REFERENCES

[1] H. A. Wafa, C. D. A. Wolfe, E. Emmett, G. A. Roth, C. O. Johnson, and Y. Wang, "Burden of Stroke in Europe: Thirty-Year Projections of Incidence, Prevalence, Deaths, and Disability-Adjusted Life Years," *Stroke,* vol. 51, no. 8, pp. 2418-2427, Aug 2020, doi: 10.1161/STROKEAHA.120.029606.

[2] A. R. Naylor *et al.*, "Editor's Choice - Management of Atherosclerotic Carotid and Vertebral Artery Disease: 2017 Clinical Practice Guidelines of the European Society for Vascular Surgery (ESVS)," *Eur J Vasc Endovasc Surg,* vol. 55, no. 1, pp. 3-81, Jan 2018, doi: 10.1016/j.ejvs.2017.06.021.

[3] D. S. Pleouras *et al.*, "Simulation of atherosclerotic plaque growth using computational biomechanics and patient-specific data," *Sci Rep,* vol. 10, no. 1, p. 17409, Oct 15 2020, doi: 10.1038/s41598-020-74583-y.

[4] A. I. Sakellarios *et al.*, "Natural History of Carotid Atherosclerosis in Relation to the Hemodynamic Environment," *Angiology,* vol. 68, no. 2, pp. 109-118, Feb 2017, doi: 10.1177/0003319716644138.

[5] N. A. Avgerinos and P. Neofytou, "Mathematical Modelling and Simulation of Atherosclerosis Formation and Progress: A Review," *Ann Biomed Eng,* vol. 47, no. 8, pp. 1764-1785, Aug 2019, doi: 10.1007/s10439-019-02268-3.

[6] A. J. Brown, Z. Teng, P. C. Evans, J. H. Gillard, H. Samady, and M. R. Bennett, "Role of biomechanical forces in the natural history of coronary atherosclerosis," *Nat Rev Cardiol,* vol. 13, no. 4, pp. 210-20, Apr 2016, doi: 10.1038/nrcardio.2015.203.

[7] A. Parton, V. McGilligan, M. O'Kane, F. R. Baldrick, and S. Watterson, "Computational modelling of atherosclerosis," *Brief Bioinform,* vol. 17, no. 4, pp. 562-75, Jul 2016, doi: 10.1093/bib/bbv081.

[8] T. Djukic, B. Arsic, I. Koncar, and N. Filipovic, "3D Reconstruction of Patient-Specific Carotid Artery Geometry Using Clinical Ultrasound Imaging," Cham, 2021: Springer International Publishing, in Computational Biomechanics for Medicine, pp. 73-83.

[9] T. Djukic, B. Arsic, S. Djorovic, N. Filipovic, and I. Koncar, "Validation of the machine learning approach for 3D reconstruction of carotid artery from ultrasound imaging," in *2020 IEEE 20th International Conference on Bioinformatics and Bioengineering (BIBE)*, 26-28 Oct. 2020 2020, pp. 789-794, doi: 10.1109/BIBE50027.2020.00134.

[10] S. A. Magder, "The highs and lows of blood pressure: toward meaningful clinical targets in patients with shock," *Crit Care Med,* vol. 42, no. 5, pp. 1241-51, May 2014, doi: 10.1097/CCM.0000000000000324.